The Plant Cell, Vol. 8, 2015–2031, November 1996 © 1996 American Society of Plant Physiologists

Spatial Organization of Calcium Signaling Involved in Cell Volume Control in the Fucus Rhizoid

Alison R. Taylor,[1] Nicholas F. H. Manison, Carlos Fernandez,[2] John Wood, and Colin Brownlee[3]

Marine Biological Association of the United Kingdom, The Laboratory, Citadel Hill, Plymouth PL1 2PB, United Kingdom

Subprotoplasts prepared from different regions of rhizoid and thallus cells of Fucus zygotes displayed mechanosensitive plasma membrane channels in cell-attached patch-clamp experiments by using laser microsurgery. In excised patches, this channel was found to be voltage gated, carrying K^+ outward and Ca^{2+} inward, with a relative permeability of Ca^{2+}/K^+ of 0.35 to 0.5, and an increased open probability at membrane potentials more positive than −80 mV. No significant difference was found in the density of this channel type from different regions of rhizoid or thallus cells. Hypoosmotic treatment of intact zygotes induced dramatic transient elevations of cytoplasmic Ca^{2+}, initiating at the rhizoid apex and propagating in a wavelike manner to subapical regions. Localized initiation of the Ca^{2+} transient correlated with greater osmotic swelling at the rhizoid apex compared with other regions of the zygote. Ca^{2+} transients exhibited a refractory period between successive hypoosmotic shocks, during which additional transients could not be elicited and the ability to osmoregulate was impaired. Buffering the Ca^{2+} transients with microinjected Br_2BAPTA similarly reduced the ability of rhizoid cells to osmoregulate. Ca^{2+} influx was associated with the initiation of the Ca^{2+} transient in apical regions, whereas intracellular sources contributed to its propagation. Thus, localized signal transduction is patterned by interactions of the cell wall, plasma membrane, and intracellular Ca^{2+} stores.

INTRODUCTION

Acquisition and expression of polarity in plant cells are fundamental processes in which cytoplasmic Ca^{2+} ($[Ca^{2+}]_{cyt}$) plays a central role. The control of polarized growth in apically growing cells, such as root hairs (Hermann and Felle, 1995), pollen tubes (Rathore et al., 1991; Miller et al., 1992; Pierson et al., 1994), and the rhizoid cell of Fucus zygotes (Brownlee and Wood, 1986; Berger and Brownlee, 1993), is dependent on the establishment and maintenance of locally elevated $[Ca^{2+}]_{cyt}$. Studies using Ca^{2+} buffer microinjections suggest that in Fucus, the $[Ca^{2+}]_{cyt}$ elevation at the rhizoid apex is required for polarization of the zygote and apical growth of the rhizoid cell (Speksnijder et al., 1989; Roberts et al., 1993).

Changes in $[Ca^{2+}]_{cyt}$ are implicated in the response of plants to a wide range of environmental, hormonal, pathogenic, and developmental signals (e.g., Gilroy et al., 1993; Poovaiah and Reddy, 1993; Ward et al., 1995). Increases in $[Ca^{2+}]_{cyt}$ in a plant cell can potentially arise either from Ca^{2+} release by intracellular organelles or via the extracellular medium. Pathways for Ca^{2+} release from vacuoles have been well characterized and occur either via voltage-activated Ca^{2+} channels (Johannes et al., 1992; Pantoja et al., 1992) or by receptor-mediated Ca^{2+} efflux (Alexandre et al., 1990; Allen et al., 1995). Ca^{2+} release channels have also been identified in the endoplasmic reticulum (Klüsener et al., 1995). Although there is now increasing evidence for voltage-activated Ca^{2+}-permeable and Ca^{2+}-selective channels in the plasma membrane that may mediate Ca^{2+} influx during signaling (see Schroeder and Thuleau, 1991; Ward et al., 1995), direct evidence linking the activity of a particular channel to a signal transduction chain by regulation of $[Ca^{2+}]_{cyt}$ is lacking. Even less is known about the coordination of Ca^{2+} influx pathways and intracellular release pathways in the regulation of $[Ca^{2+}]_{cyt}$ in plants.

In patch-clamp studies, several mechanosensitive or stretch-activated channels (SACs) conducting Ca^{2+} in the plant plasma membrane have been described (Cosgrove and Hedrich, 1991; Ding and Pickard, 1993). These studies raise the possibility that the channels may also regulate Ca^{2+} influx during transduction of certain signals, although a clear demonstration of their function in the intact cell remains obscure because an unambiguous link between Ca^{2+}-permeable SACs and $[Ca^{2+}]_{cyt}$ has not been demonstrated. SACs that are localized in the plasma membrane of fungal hyphal tips have also been described (Garrill et al., 1992); however, in these studies, the inability to obtain whole-cell or single-channel recordings in excised patches has precluded determining their selectivity.

[1] Current address: Department of Vegetable Crops, University of California at Davis, Davis, CA 95616.

[2] Current address: Lawrence Berkeley Laboratory, 1 Cyclotron Road, Berkeley, CA 94720.

[3] To whom correspondence should be addressed.

In this study, UV laser microsurgery was refined so that plasma membrane patch–clamp recordings could be made from localized regions of the polarized Fucus zygote. Measurements of intracellular Ca^{2+} using ratio photometric and imaging techniques were used to monitor changes in Ca^{2+} in response to activation of the channels characterized by patch clamping. This study demonstrates that stretch-activated Ca^{2+}-permeable channels in the plasma membrane of polarized Fucus zygotes underlie spatial signaling involving localized increases of $[Ca^{2+}]_{cyt}$ in response to changes in cell volume. Furthermore, at least two pathways of Ca^{2+} entry into the cytoplasm appear to be involved in signal transduction in the rhizoid cell.

RESULTS

UV Laser Microsurgery and Localized Patch Clamping of Fucus Rhizoid and Thallus Cells

In this study, protoplasts were extruded through a hole cut in the cell wall with a UV laser by applying gentle mechanical pressure to the zygote with a polished glass electrode (Figures 1A and 1C). This offered advantages over osmotic protoplast extrusion (Figure 1B) (Taylor and Brownlee, 1992) because the timing of extrusion could be accurately controlled, the size of the protoplast was easily varied according to requirements, and the external medium did not change during protoplast extrusion and remained well defined. An average seal resistance of 4.8 GΩ (±0.4; n = 268) was achieved on laser-isolated protoplasts from both rhizoid and thallus regions. Channel activity was observed in 82% (n = 180) of the patches derived from rhizoid tip protoplasts and in 85% (n = 54) from thallus protoplasts. There was no significant difference in the total number of channels per active patch (2.48 ± 0.16 and 2.7 ± 0.28 for the rhizoid apex and thallus, respectively), indicating no gross differences in channel distribution between the rhizoid apex and thallus cells.

SACs in the Plasma Membrane of Fucus

Figure 2A shows that application of negative pressure (0.5 to 2 kPa) to the pipette holder in a cell-attached configuration caused an increase in channel activity. This could be observed in 70% of the patches (n = 40) at all of the pipette potentials studied. SACs were observed in a cell-attached configuration from both the thallus (15 of 18 recordings) and rhizoid regions (15 of 22 recordings). Mechanosensitivity of channels was not observed in excised patches. Figure 2B shows that an increase in the probability of opening (P_{open}) values is not due to an increase in channel incorporation via membrane recruitment into the patch. In this case, increases in P_{open} values of the single small and large conductance channels were observed during stretch activation, without additional open levels being detected. In the case of the large conductance channel, dual openings would have been expected with a probability of 0.23 if a second channel were incorporated into the patch during suction.

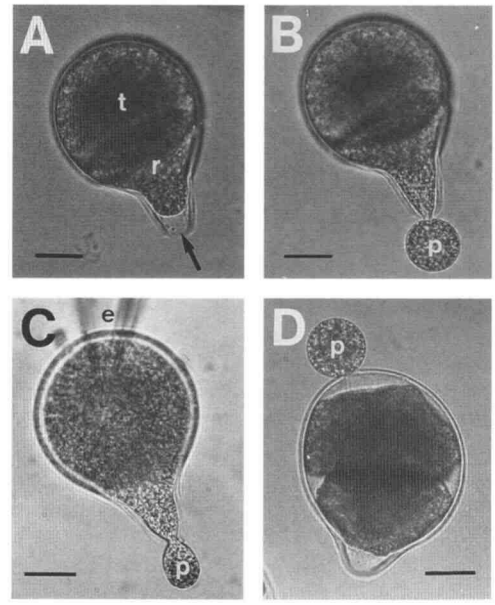

Figure 1. Protoplast Production from Fucus Zygotes by UV Laser Ablation of the Cell Wall.

(A) Shown is a 24-hr-old zygote with thallus (t) and rhizoid (r) cells after plasmolysis with ASW plus 1 M sorbitol. The cytoplasm has receded sufficiently within the rhizoid compartment to enable laser ablation of the cell wall (arrow).

(B) After cell wall ablation, reduction of extracellular osmolarity causes the thallus and rhizoid cells to expand within the cell wall. A rhizoid tip protoplast (p) is extruded through the laser-ablated hole.

(C) A polished electrode (e) is manipulated to apply gentle mechanical pressure on the thallus cell to produce a rhizoid tip protoplast (p). Most of the electrode appears out of focus because of the steep angle of the approach.

(D) The laser microsurgery technique can be used to isolate protoplasts (p) from the thallus cell.

Bars = 20 μm.

Ca^{2+} Permeability and Voltage Sensitivity of Mechanosensitive Channels

A more detailed analysis of plasma membrane channels in an excised (inside-out) configuration revealed that the channels observed in cell-attached recordings were cation channels that are permeable to Ca^{2+}. Figure 3 shows single-channel current–voltage (I/V) curves recorded with varying pipette solutions designed to determine the permeability of the cation

channels to Ca^{2+} and K^+ (see Table 1 for summary). Where stretch activation was tested in a cell-attached configuration before excision, I/V plots are marked with open symbols in Figure 3. Figure 3A shows that with 30 mM K^+ as the only cation in the bath and pipette, the single-channel current reversed at E_{K+} (−45 mV) with a mean conductance of 110 pS. With a pipette solution of 30 mM KCl and 30 mM Ca^{2+}, added either as the glutamate or chloride salt, the reversal potential (E_{rev}) estimated from the mean I/V plot shifted 14 and 11 mV positive of E_{K+} (−47 mV), respectively, giving an estimated permeability ratio of $P_{Ca^{2+}}/P_{K^+}$ of 0.05 and 0.39 (Figures 3B and 3C, respectively). Channel conductance was reduced to 58 and 62 pS in the presence of 30 mM Ca^{2+} in the pipette for Cl^- and glutamate salts, respectively. The Ca^{2+} permeability of the cation channel was confirmed in experiments in which E_{K^+} was set more negative by reduction in the pipette [K^+]. Single-channel I/V plots obtained with 30 mM $CaCl_2$ and 0.5 mM KCl in the pipette reversed 92 mV more positive of E_{K^+} (−149 mV), giving an estimated $P_{Ca^{2+}}/P_{K^+}$ ratio of 0.38 (Figure 3D). Smaller conductance channels were observed less frequently and also exhibited Ca^{2+} permeability (Figure 3E). Only a small positive shift of 3 mV from E_{K^+} (−74 mV) was detected when Mn^{2+} was substituted as the divalent cation in the pipette, giving an estimated permeability ratio of $P_{Mn^{2+}}/P_{K^+}$ of 0.025 (Figure 3F).

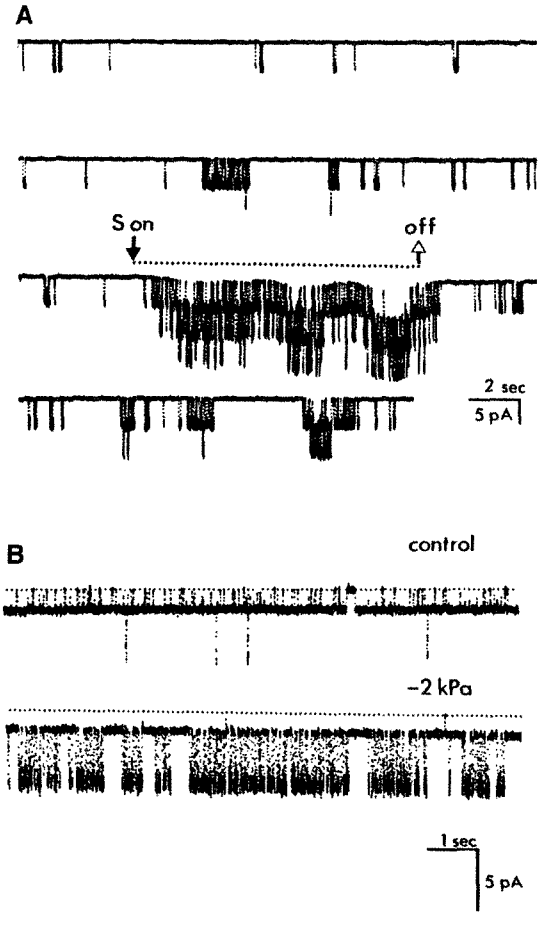

Figure 2. Mechanosensitive Channels in the Fucus Plasma Membrane.

(A) Cell-attached recording from a subapical rhizoid location showing spontaneous inward channel activity at an assumed membrane potential of −70 mV (V_{mem} of −60 mV; pipette voltage of +10 mV). Application of a stretch stimulus (−1.5 kPa; arrow and dotted line) caused a significant increase in channel activity, which decreased when stimulation ended. The P_{open} value before suction was 0.03, and it increased to 0.42 during stretch activation.

(B) Cell-attached recording from an apical rhizoid location showing stretch activation of individual high- and low-conductance channels. The P_{open} values for the small and large conductance channels were 0.96 and 0.05, respectively, before stretch activation (upper trace) and 1.0 and 0.48, respectively, during stretch activation (lower trace). The dotted line represents the level at which both channels are closed. Pipette solutions contained 200 mM potassium–glutamate in **(A)** and **(B)**.

Altering the [Cl^-] at the extracellular face did not shift E_{rev} values in the direction that would be predicted if the channel were significantly permeable to anions. For example, in Figure 3A, assuming a low permeability to glutamate, E_{Cl^-} (approximately −140 mV) is very negative of E_{K^+} (−44 mV); a more negative E_{rev} value would be expected if the channel were significantly permeable to Cl^-. Likewise, a change in the [Cl^-] at the extracellular side of the patch by the addition of 30 mM $CaCl_2$ would shift the E_{rev} value negatively and not positively if the channel were significantly permeable to Cl^-. The latter argument applies also if significant permeability to both Cl^- and glutamate is considered. The observation that the addition of external Ca^{2+} ($[Ca^{2+}]_{ext}$) in the presence of Cl^- or glutamate salt causes a positive shift in E_{rev} values from E_{K^+} demonstrates that this channel has no significant anion permeability.

All of the channels recorded were voltage activated in either a cell-attached or excised-patch configuration, showing an increase in P_{open} values as the patch was depolarized. Figure 4A illustrates current traces for channels recorded at different voltages with 30 mM $CaCl_2$ and 0.5 mM KCl in the pipette. Figure 4B shows the mean P_{open} for all channels recorded in experiments with 30 mM $CaCl_2$ and 0.5 mM KCl (see Figure 3D) plotted against membrane voltage (V_{mem}) and fitted with a Boltzmann function, as described in the legend of Figure 4. Verapamil or nifedipine did not affect P_{open} or channel conductance when applied to either face of the membrane at concentrations up to 10^{-4} M. Open circles in Figure 4B show P_{open} values in the presence of 5×10^{-5} M verapamil.

Ca^{2+}-permeable cation channels were completely and reversibly blocked by 0.5 mM Gd^{3+} on the cytoplasmic (n = 8; Figures 5A and 5B) and the extracellular (data not shown) face. Partial block by 1 mM tetraethylammonium was also observed (data not shown). Channel run-down was frequently observed after excision as single-channel activity declined 10 sec to 5 min after excision.

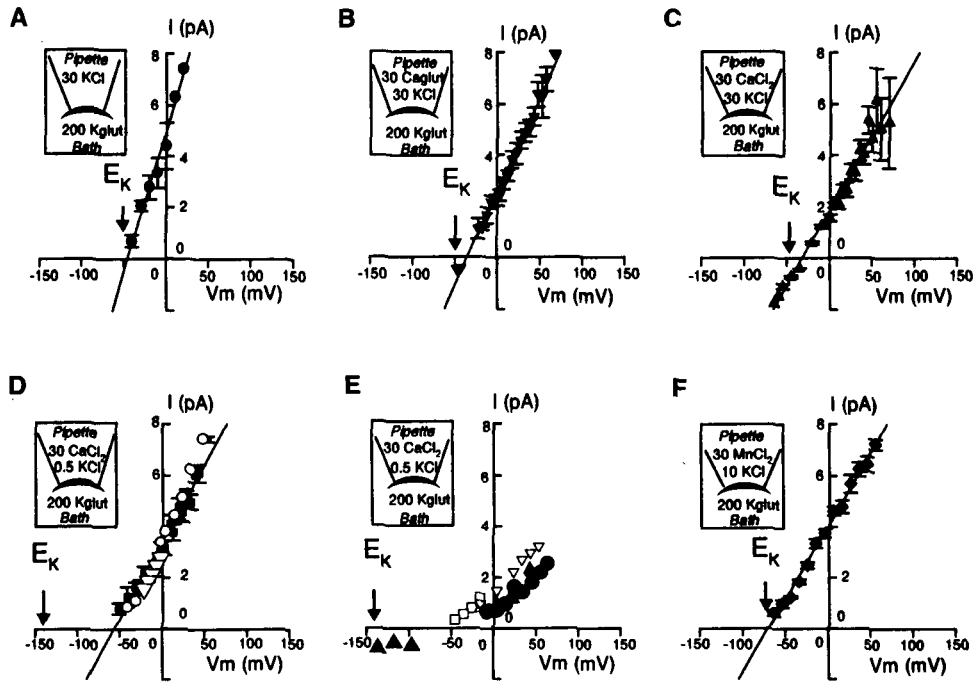

Figure 3. *Permeability of Mechanosensitive Cation Channels in the Fucus Rhizoid Plasma Membrane.*

Details of all solutions, E_{K^+}, and summaries of permeability ratios are given in Table 1. Closed symbols in **(A)** to **(F)** represent recordings made in excised inside-out membrane patches. Different symbols represent recordings from different cells. In **(D)** and **(E)**, open symbols represent channels in excised patches that had been previously stretch-activated in cell-attached recording configuration. Caglut, calcium glutamate; Kglut, potassium glutamate; Vm, membrane holding potential.

(A) With K^+ as the only permeant cation, the mean single-channel conductance was 110 pS and $E_{rev} = E_{K^+}$ (−45 mV).

(B) With equimolar potassium glutamate and $CaCl_2$ in the pipette, the mean conductance was reduced to 72 pS, and E_{rev} values were shifted positive of E_{K^+} to −35.5 mV, giving an estimated $P_{Ca^{2+}}/P_{K^+}$ ratio of 0.39.

(C) With equimolar KCl and $CaCl_2$ in the pipette, the mean conductance was 58 pS, and the E_{rev} value was shifted positive of E_{K^+} to −32.45 mV, giving an estimated $P_{Ca^{2+}}/P_{K^+}$ ratio of 0.5.

(D) With 30 mM $CaCl_2$ and 0.5 mM KCl in the pipette, the mean conductance was 60 pS, and the E_{rev} value (−56.5 mV) was shifted positive of E_{K^+}, giving an estimated P_{K^+}/P_{K^+} ratio of 0.38.

(E) A small conductance (23 pS) Ca^{2+}-permeable cation channel was observed less frequently. The E_{rev} value was positive of E_{K^+} and gave an estimated $P_{Ca^{2+}}/P_{K^+}$ ratio of ~0.4.

(F) With 30 mM $MnCl_2$ and 10 mM KCl in the pipette, single-channel conductance was 57 pS, and the mean E_{rev} value of −70.7 mV was only slightly positive of E_{K^+}, giving a $P_{Mn^{2+}}/P_{K^+}$ ratio of 0.025.

Localized Transient Increases in Cytoplasmic Ca^{2+} in Response to Osmotic Shock

Mean resting $[Ca^{2+}]_{cyt}$ in rhizoid cells bathed in artificial seawater (ASW; 450 mM NaCl, 10 mM KCl, 10 mM $CaCl_2$, 30 mM $MgSO_4$, and 2.5 mM $NaHCO_3$) plus 0.7 M sorbitol was uniform, with a mean value of 139 nM (n = 41; ±30 nM). Transfer from ASW plus 0.7 M sorbitol to normal ASW elicited a dramatic transient elevation in $[Ca^{2+}]_{cyt}$ at the rhizoid apex in 89% of the cells examined (n = 39; Figure 6A). The $[Ca^{2+}]_{cyt}$ transient typically lasted for 60 to 120 sec, reaching values of >1 μM before returning to a resting level close to or slightly higher than the initial level (Figure 6A). The increase in Ca^{2+} was clearly localized to the apex of the rhizoid. Measurements taken in subapical regions (at least 20 μm from the apex; Figure 6B) showed only a small transient increase in $[Ca^{2+}]_{cyt}$ (mean = 550 nM ±20; n = 7). On returning to the hyperosmotic solution, an additional small increase in $[Ca^{2+}]_{cyt}$ was observed at the rhizoid apex. Larger transient changes in $[Ca^{2+}]_{cyt}$ could be induced by transfer to more hyperosmotic solutions. Ratio imaging of fura-2–loaded zygotes during hypoosmotic shock clearly showed uniformly low $[Ca^{2+}]_{cyt}$ in the hyperosmotic medium (ASW plus 0.5 M sorbitol). An increase in $[Ca^{2+}]_{cyt}$ was initiated at the extreme rhizoid apex (Figure 7B) and spread to subapical regions as the rhizoid swelled in response to hypoosmotic shock (n = 6; Figures 7C and 7D). In the experiment shown, a more severe osmotic shock was administered (ASW plus 0.5 M sorbitol to 50% ASW),

and the Ca^{2+} transient was more prolonged, lasting >100 sec. Apically elevated Ca^{2+} was observed upon return to ASW (Figure 7E). No change in $[Ca^{2+}]_{cyt}$ was observed in thallus cells in response to hypoosmotic shock. Normal rhizoid growth was observed upon return to ASW after both hyperosmotic and hypoosmotic treatments (data not shown).

Transfer of zygotes from a plasmolyzing solution (1.2 M sorbitol plus 50% ASW) to 50% ASW produced a Ca^{2+} transient, which decayed only slowly to a higher resting value (Figure 8A). In the results of the experiment shown, transfer back to the plasmolysis solution elicited a small transient followed by a larger Ca^{2+} transient as the plasma membrane receded from the cell wall. Figure 8B shows the effect of plasmolysis on the Fucus zygote. The plasma membrane and cytoplasm recede and pull away from the cell wall. Cytoplasmic strands appear in the apical region of the plasmolyzed rhizoid, which remain attached to the cell wall at discrete points. The increase in $[Ca^{2+}]_{cyt}$ associated with perfusion of the hyperosmotic solution coincided with the onset of acute plasmolysis of the cytoplasm.

Differential Osmotic Swelling in Rhizoid and Thallus

On transfer from hyperosmotic to hypoosmotic solution, swelling of the rhizoid cytoplasm could be observed ~10 sec before the onset of the Ca^{2+} transient, which was initiated only when the cytoplasm expanded to fill the cell wall cavity (Figure 9A). Measurements of cell diameter and calculated surface area and volume changes during hypoosmotic shock showed that the rhizoid tip swells more than the thallus does, suggesting that the plasma membrane at the apex of the rhizoid is subject to greater mechanical stress than in subapical and thallus regions (Figure 9B).

Refractory Period of Hypoosmotically Induced $[Ca^{2+}]_{cyt}$ Transients and Osmoregulation

To determine whether the Ca^{2+} transients showed desensitization in response to hypoosmotic shock, we subjected zygotes to a double-shock protocol with a variable interval between shocks. The transient responses in $[Ca^{2+}]_{cyt}$ induced by hypoosmotic shock exhibited a refractory period. During this period, additional transients could not be elicited in response to a second, greater hypoosmotic shock. Figure 10A illustrates $[Ca^{2+}]_{cyt}$ monitored at the apex of a rhizoid in response to consecutive hypoosmotic shocks (peaks a to d). Changing the bath perfusion from ASW plus 0.5 M sorbitol to ASW initiated a large Ca^{2+} transient at the rhizoid apex (peak a). Subjecting the zygote to a second hypoosmotic shock (ASW into 50% ASW) 300 sec after the first failed to elicit a second Ca^{2+} transient (peak b). Transfer to ASW after the first hypoosmotic shock for 10 min followed by a second hypoosmotic shock (ASW to 50% ASW) produced a small transient (peak c). A period of up to 30 min was required after the first shock before a second full Ca^{2+} transient could be elicited (peak d).

Ca^{2+} Transients and Osmoregulation

The role of the Ca^{2+} transient in the regulation of cell volume during hypoosmotic shock was investigated by using a two-shock protocol and Ca^{2+} buffer microinjection. Zygotes treated with an osmotic shock every 30 min or more could withstand the shock. Zygotes subjected to a double osmotic shock within the refractory period for the Ca^{2+} transient response showed an increased frequency of rupturing at the rhizoid apex (Figure 10C), that is, they showed a reduced ability to osmoregulate after the second hypoosmotic shock (Figure

Table 1. Extracellular and Cytoplasmic[a] Solution Compositions and Ion Activities (α_{ion}) for Determining the Ca^{2+}/K^+ Selectivity in Single Channels in Excised Inside-Out Patches

	Extracellular (Pipette) Solution (mM)				
Solution Composition/ Ion Activity	30 KCl	30 KCl + 30 Ca-glutamate	30 KCl + 30 $CaCl_2$	0.5 KCl + 30 $CaCl_2$	10 KCl + 30 $MnCl_2$
αK^+ extracellular (mM)	25.4	22.7	22.7	0.39	0.39
αCa^{2+} or αMn^{2+} extracellular (mM)	0	9.9	9.9	11	10.6
E_{K^+} (mV)	−44.6	−46.8	−46.8	−149	−74
E_{rev} from I/V plots (Figure 3) (mV)	−45	−35.5	−32.4	−56.5	−70.7
LJP (mV)	−14	−11	−13	−17	−15
Permeability ratio $P_{Ca^{2+}}/P_{K^+}$	—	0.36	0.50	0.35	0.025
Conductance (pS)	110	62	58	60	57
No. of experiments	7	9	8	14	14
Figure reference	3A	3B	3C	3D	3F

[a] Cytoplasmic K^+ activity (αK^+) = 144 mM; αCa^{2+}_{cyt} = 5 nM.

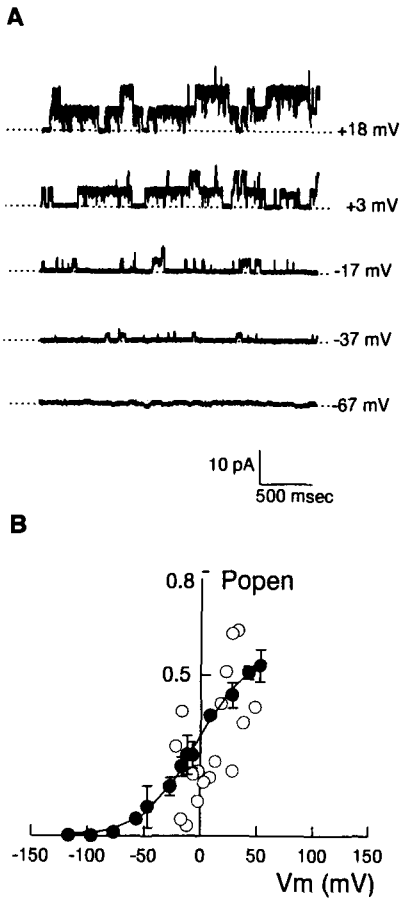

Figure 4. Voltage Dependence of Mechanosensitive Channels.

(A) An example of channels recorded in an excised configuration showing an increase in P_{open} values with membrane depolarization. The pipette contained 0.5 mM KCl and 30 mM $CaCl_2$, and the bath solution contained 200 mM potassium glutamate.

(B) Mean P_{open} values for all of the recordings in Figure 3D plotted against voltage (closed circles). A Boltzmann curve was fitted to the data (see Methods for details). For the data presented, $V_{0.5} = -4.4$ mV, $P_{open^{max}} = 0.57$, and S has a value of 23.3 mV ($\delta = 1$). Open circles show the same channels in the presence of 5×10^{-5} M verapamil.

10B). Microinjection of the Ca^{2+} buffer Br_2BAPTA also reduced the ability of zygotes to osmoregulate (Figure 11). Intracellular [Br_2BAPTA] >5 mM significantly increased the percentage of zygotes that burst in response to a single hypoosmotic shock. All Br_2BAPTA-injected cells that burst in response to hypoosmotic treatment also failed to generate Ca^{2+} transients (data not shown). Nifedipine or verapamil at concentrations up to 5×10^{-5} M did not inhibit the Ca^{2+} transient response and did not affect the ability of zygotes to osmoregulate (data not shown).

Ca^{2+} Influx during Hypoosmotic Shock

In the extreme apex (10 μm) of the rhizoid cell, Ca^{2+} influx, monitored by the Mn^{2+}-quenching technique, could be detected simultaneously with the onset of the Ca^{2+} transient during hypoosmotic shock (Figure 12A; $n = 4$). The Ca^{2+} influx was restricted to the rising phase of the Ca^{2+} transient. In contrast, when the isosbestic fura-2 fluorescence signal was recorded from the apical and subapical 40 μm of the rhizoid cell and when it represented predominantly fluorescence from

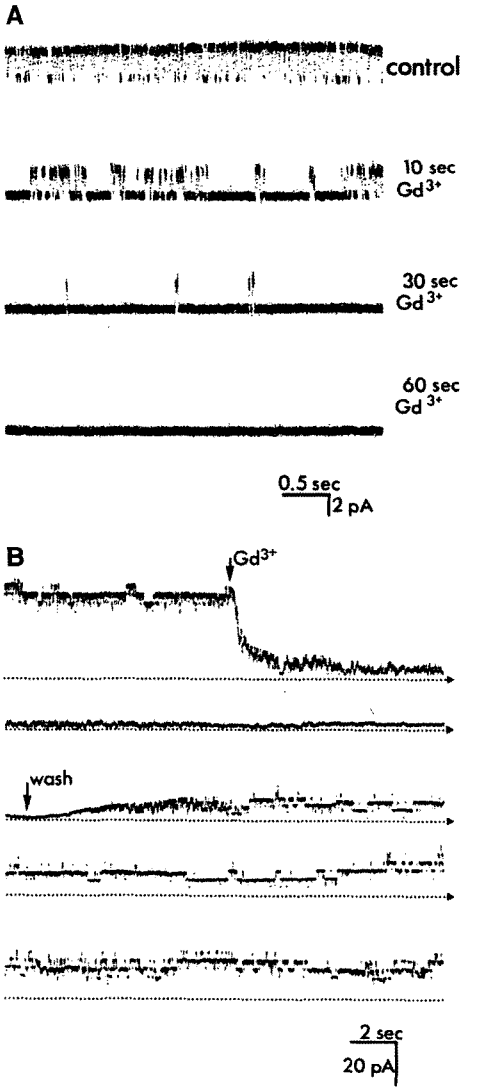

Figure 5. Gd^{3+} Block of a Ca^{2+}-Permeable Channel.

(A) Excised patch with a V_{mem} of +20 mV with one active channel. The channel was completely blocked after bath perfusion with 0.5 mM Gd^{3+}.

(B) Recording from a multichannel patch. The dotted line indicates the current level at which all of the channels were inactive. Bath perfusion with 0.5 mM Gd^{3+} (arrow) reversibly blocked all of the channels.

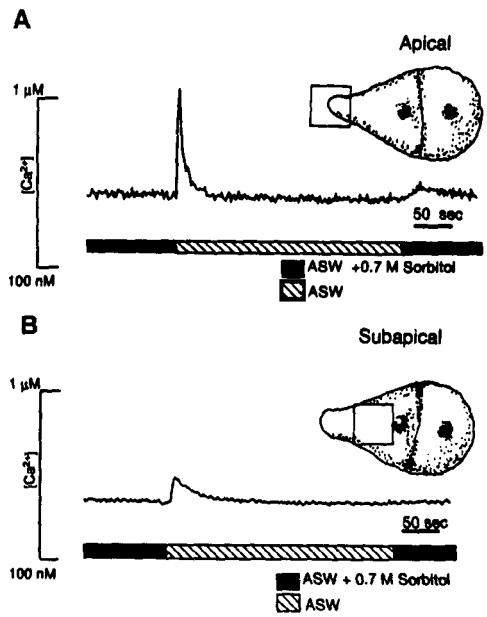

Figure 6. Changes in $[Ca^{2+}]_{cyt}$ in Response to Hypoosmotic Shock in Apical and Subapical Rhizoid Regions.

Zygotes loaded with fura-2–dextran were preincubated in ASW plus 0.7 M sorbitol for 1 hr. This reduced cell turgor without causing severe plasmolysis. Boxes in **(A)** and **(B)** define regions from which recordings were made.

(A) Bath perfusion with ASW elicited a rapid transient increase in $[Ca^{2+}]_{cyt}$ in the apical (0- to 20-μm) region within 10 sec of solution change.

(B) The subapical (20- to 50-μm) region showed a smaller transient increase in $[Ca^{2+}]_{cyt}$ in response to the same hypoosmotic shock.

subapical regions, Ca^{2+} influx was only detected after the completion of the Ca^{2+} transient (Figure 12B; $n = 5$).

Gd^{3+} Inhibition of the Ca^{2+} Transient and Osmotic Swelling

Transfer of zygotes from ASW to 50% ASW consistently induced a small transient increase in rhizoid cell volume (Figure 13A), returning to the initial volume after ~2 to 3 min ($n = 4$). When returned to ASW, a significant decrease in cell volume occurred, reaching a value less than the initial value in ASW (Figure 13A). The changes in cell volume in response to this hypoosmotic shock were associated with a transient increase in $[Ca^{2+}]_{cyt}$ in the rhizoid apex (Figure 13B). Figure 13B also shows that fluorescence at the Ca^{2+}-independent isosbestic excitation wavelength (360 nm) changed only slightly during the Ca^{2+} transient, confirming that the changes in fluorescence ratio in response to osmotic treatments were not due to altered optical properties of the cell. In the presence of 3 mM Gd^{3+}, however, the degree and rate of osmotic swelling were significantly reduced (Figure 13C). Gd^{3+} also abolished the Ca^{2+} transient in response to hypoosmotic shock (Figure 13D). Gd^{3+} protected zygotes from bursting. Osmotic bursting was induced by administering two consecutive hypoosmotic shocks within 5 min. Control cells showed a 26% (±7; $n = 4$) rate of bursting in response to this treatment; this rate was reduced to 9% (±7; $n = 4$) in the presence of 5 mM Gd^{3+}.

DISCUSSION

Protoplast Isolation by Laser Microsurgery

The laser microsurgery technique (Taylor and Brownlee, 1992) has been refined to allow rapid production of plasma membrane–bound protoplasts from localized regions of the Fucus zygote. Intact protoplasts derived from thallus and rhizoid regions have normal V_{mem} values, begin to form a new cell wall within 20 min, and, when nucleated, are developmentally competent, forming a new polarized zygote within 24 hr (Berger et al., 1994; Berger and Brownlee, 1995). In this study, controlled mechanical extrusion permitted rapid isolation (within a few seconds) of protoplasts in a well-defined extracellular medium. The high success rate of seal formation on the laser-isolated protoplasts has enabled a detailed study of plasma membrane channels in the developing zygote. Laser-assisted protoplast isolation has been attempted with other algal (DeBoer et al., 1994) and higher plant cells (Kurkdjian et al., 1993; DeBoer et al., 1994), and successful patch clamping of the guard cell plasma membrane after laser microsurgery has recently been demonstrated (Henricksen et al., 1996). With continued refinements, the technique should prove valuable in various cell types in which enzymatic digestion of the cell wall is neither desirable nor achievable and in which patch-clamp data from defined cell types or regions of a single cell are required.

Ca^{2+} Permeability of the Plasma Membrane Cation Channel

Ca^{2+} permeability has been characterized using the conventional method whereby the effect of ion substitution on the reversal (or zero channel current) potential of the single-channel I/V relationship is determined. Ca^{2+}-selective plasma membrane channels have been described for a few plant cell types, including wheat root (Piñeros and Tester, 1995) and carrot suspension-cultured cells (Thuleau et al., 1994), and it is thought that they play an essential role in the regulation of $[Ca^{2+}]_{cyt}$ during signal transduction. An alternative pathway for Ca^{2+} entry into the cytosol during signaling events is via Ca^{2+} permeation of nonselective cation channels (Schroeder and Hagiwara, 1990). Ca^{2+} permeation of inward K^+ rectifier channels has also been characterized in the plasma membrane

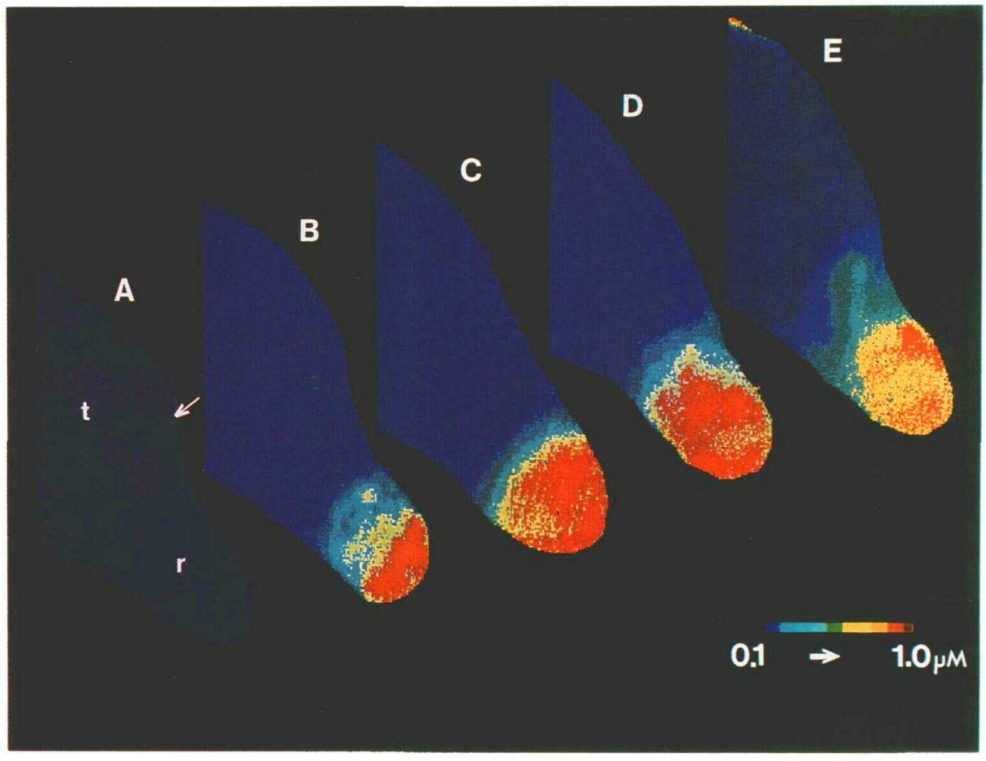

Figure 7. Ratio Images of $[Ca^{2+}]_{cyt}$ in a Fura-2–Loaded Zygote in Response to Hypoosmotic Shock.

(A) Resting cell preincubated for 1 hr in ASW plus 0.5 M sorbitol. The rhizoid (r), thallus (t), and plane of cell division (arrow) are indicated. **(B)** to **(D)** $[Ca^{2+}]_{cyt}$ elevation originating at the rhizoid apex and spreading to subapical rhizoid regions after external perfusion with 50% ASW for 20 **(B)**, 50 **(C)**, and 100 **(D)** sec.

(E) The same cell 30 min after transfer to ASW, showing elevated $[Ca^{2+}]_{cyt}$ in the apical rhizoid region. The thallus cell shows no change in $[Ca^{2+}]_{cyt}$ during hypoosmotic shock.

of the guard cell (Fairley-Grenot and Assmann, 1992). In that study, the $P_{Ca^{2+}}/P_{K^+}$ ratios were dependent on both $[Ca^{2+}]_{cyt}$ and $[Ca^{2+}]_{ext}$ with a $P_{Ca^{2+}}/P_{K^+}$ ratio of 0.3 with 10 mM extracellular Ca^{2+} and K^+, which also approximates the availability of these ions in seawater. The slow vacuolar channel of the guard cell vacuolar membrane is weakly selective for Ca^{2+} with a $P_{Ca^{2+}}/P_{K^+}$ ratio of 3:1 (Ward and Schroeder, 1994; Allen and Sanders, 1995). Thus, several channels permeable to Ca^{2+} have been described that range from relatively nonselective or Ca^{2+} permeable to strongly Ca^{2+} selective. In our study, the permeability ratios with respect to K^+ show a permeability sequence of $K^+ > Ca^{2+} >> Mn^{2+}$. With $[Ca^{2+}]_{ext}$ (in seawater) of 9 mM and resting $[Ca^{2+}]_{cyt}$ in the nanomolar range, there is a steep gradient favoring Ca^{2+} influx through these cation channels when they are activated. Few data are available on the permeability of plant channels to Mn^{2+}. In wheat root plasma membrane, voltage-dependent Ca^{2+}-selective channels are 45% permeable to Mn^{2+} based on unitary conductance (Piñeros and Tester 1995), and in the red beet vacuole, voltage-dependent Ca^{2+} channels permit passage of Mn^{2+} but the P_{open} value is much reduced (Johannes and Sanders, 1995). Our data show that the Ca^{2+}-permeable cation channel is not blocked by Mn^{2+} but has a low permeability to Mn^{2+}.

Voltage Sensitivity and Mechanosensitivity of the Ca^{2+}-Permeable Cation Channel

The Ca^{2+}-permeable cation channel is voltage activated, increasing in activity with a V_{mem} more positive than −80 mV, with half-maximal activation ($V_{0.5}$) of −4 mV and a slope factor (S) of 24 mV. Interestingly, these are comparable to the steady state activation kinetics of the stomatal guard cell K^+ outward rectifier in which $V_{0.5}$ and S have values of −7 and 21 mV, respectively (Schroeder, 1989). The cations can permeate in both inward and outward directions because inward currents are observed when the V_{mem} value is more positive

than the activation threshold for the channel but negative of E_{K^+}. This is likely to be the case under physiological conditions (10 mM $[Ca^{2+}]_{ext}$ and 10 mM $[K^+]_{ext}$, where E_{rev} would be close to −50 mV [Jan and Jan, 1976]). Moreover, assuming independent ion movement through the channels, then Ca^{2+} influx should still occur even when the net current is outward. The resting V_{mem} value of the Fucus zygote is −80 mV in normal seawater and follows a Nernstian relationship with respect to extracellular K^+ (Taylor and Brownlee, 1993). Unlike most higher plant cells, there is no evidence that an electrogenic pump contributes significantly to V_{mem} values in Fucus (Gibbon and Kropf, 1994); thus, it is likely that the cation channel characterized here plays an important role in regulating V_{mem}.

Stretch-activated Ca^{2+}-selective channels in guard cells (Cosgrove and Hedrich, 1991), onion epidermal cells (Ding and Pickard, 1993), red beet vacuoles (Alexandre and Lassalles, 1990), and yeast cells (Gustin et al., 1986) may contribute to $[Ca^{2+}]_{cyt}$ regulation during signaling responses to a wide range of mechanical and osmotic stimuli. The high frequency of SACs observed in Fucus plasma membrane would be expected for a zygote of an intertidal alga that is subject to rapid and extreme changes in osmotic conditions if these mechanosensitive channels contribute to solute fluxes during osmotic stress. In addition, the Ca^{2+} permeability of mechanosensitive channels characterized here suggests a role for regulation of $[Ca^{2+}]_{cyt}$ during both typical growth and osmotic stress. This hypothesis has been supported by monitoring $[Ca^{2+}]_{cyt}$ during osmotic treatments that would result in SAC activation.

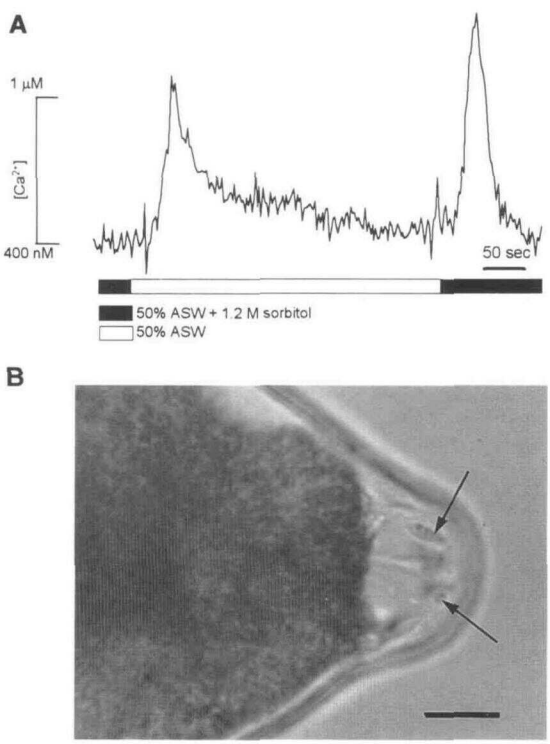

Figure 8. Ca^{2+} Transients in Response to Severe Hypoosmotic and Hyperosmotic Shock.

(A) Changing from a hyperosmotic medium (preincubation for 3 hr in 50% ASW plus 1.2 M sorbitol) to 50% ASW elicited a Ca^{2+} transient that decayed slowly to a higher resting $[Ca^{2+}]_{cyt}$. Transfer back to a hyperosmotic solution after 20 min induced a second Ca^{2+} transient in response to plasmolysis.

(B) Cytoplasmic adhesions at the rhizoid apex remain attached to the cell wall (indicated by arrows) during plasmolysis. Bar = 10 μm.

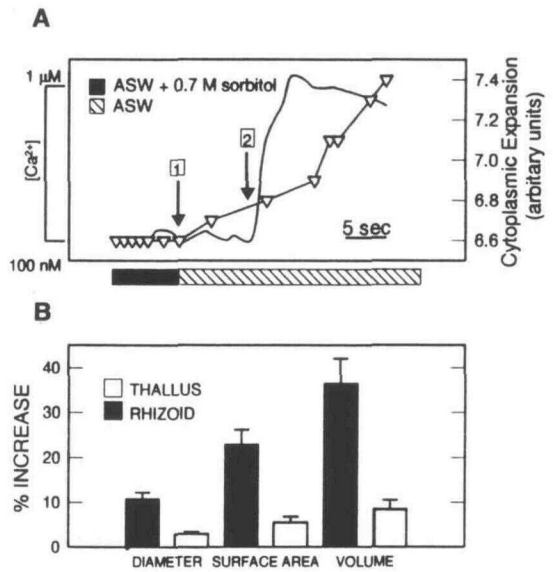

Figure 9. Time Course for Cytoplasmic Swelling during Hypoosmotic Shock of a Partially Plasmolyzed Rhizoid Cell.

(A) The cell was preincubated in 0.7 M sorbitol for 1 hr and perfused with ASW at arrow 1. Cytoplasmic swelling in the rhizoid apex began before the onset of the Ca^{2+} transient. The Ca^{2+} transient was triggered after the cytoplasm expanded to fill the cell wall cavity completely (arrow 2).

(B) Changes in the dimensions of rhizoid cells in response to hypoosmotic shock were calculated from the change in the rhizoid diameter measured 10 μm from the rhizoid apex. Changes in the diameter of the thallus cell were measured in the equatorial plane of that cell. Diameters were measured before and 1 min after hypoosmotic shock. Cell diameter increased significantly more at the rhizoid apex. Bars indicate SE.

Distribution and Activation of Ca^{2+}-Permeable Cation Channels in the Fucus Zygote

It has been proposed that the asymmetric distribution of plasma membrane Ca^{2+} channels could account for both inward currents detected with the extracellular vibrating probe and generation of intracellular Ca^{2+} gradients in the apical tip of

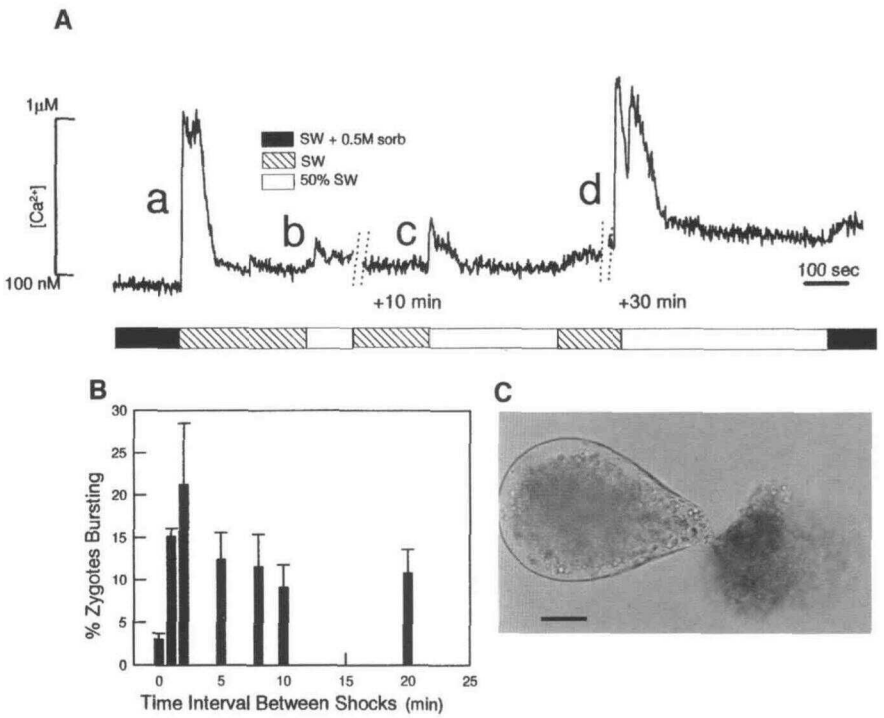

Figure 10. Ca^{2+} Transients and Osmoregulation in Response to Successive Hypoosmotic Shocks.

(A) Ca^{2+} transients measured in the rhizoid apex (0 to 30 μm). Peak a shows the Ca^{2+} transient's response to a single hypoosmotic shock from ASW plus 0.5 M sorbitol (sorb) to ASW. Peak b shows the results of a second shock (from ASW into 50% ASW) given within 5 min of the first shock that failed to elicit a second transient. Peak c shows the result of transfer from ASW into 50% ASW after an additional 12 min that elicited a small Ca^{2+} transient. Peak d shows a full Ca^{2+} transient in the same cell in response to hypoosmotic shock given after an additional 40 min.
(B) Variation in the ability of zygotes to osmoregulate in response to different time intervals between two successive hypoosmotic shocks (shock 1 of ASW plus 0.5 M sorbitol into ASW; shock 2 of ASW into 50% ASW). The reduced ability to osmoregulate was monitored as an increase in the number of zygotes in populations of >100 zygotes that burst in response to the second shock **(C)**. A second shock given immediately after the first shock did not increase the incidence of bursting. Error bars indicate standard deviation. The inability to osmoregulate increased significantly as the interval between shocks was increased up to 5 min and declined thereafter.
(C) Cells unable to osmoregulate burst at the apex of the zygote where the cell wall is weakest. Bar = 20 μm.

Pelvetia and Fucus rhizoids (reviewed in Kropf, 1994), root hairs (Hermann and Felle, 1995), pollen tubes (Steer and Steer, 1989; Pierson et al., 1994; Feijo et al., 1995), and fungal hyphae (Garrill et al., 1992). A recent study using fluorescently labeled dihydropyridine (DHP) in polarizing Fucus zygotes showed preferential labeling at the rhizoid pole (Shaw and Quatrano, 1996), suggesting an asymmetric distribution of DHP receptors, although the specificity of this labeling for Ca^{2+} channels in the Fucus rhizoid has not been determined. We detected no significant difference in distribution of the mechanosensitive, voltage-activated Ca^{2+}-permeable channel characterized in this study. The insensitivity of this channel to nifedipine or verapamil suggests that this is not the same channel as that proposed to bind to fluorescent DHP (Shaw and Quatrano, 1996). It is unlikely that any asymmetry in channel distribution would be lost due to the hyperosmotic treatments used in this study because the apical Ca^{2+} gradient returns and growth resumes on return to normal seawater.

The evidence given above raises the possibility that channel gating may be spatially regulated in the Fucus rhizoid. As with other apically growing cells, fucoid rhizoid extension is believed to be driven by turgor pressure. Fucoid zygotes develop turgor pressure (Allen et al., 1970) at about the same time after fertilization as actin localization at the rhizoid pole during zygote polarization (Kropf et al., 1989). Softening of the cell wall, increased cell wall secretion, and transcellular currents have been detected at the presumptive rhizoid pole (Kropf, 1992). A Ca^{2+} gradient develops just before rhizoid germination (Berger and Brownlee, 1993) and is maintained throughout typical rhizoid development (Brownlee and Wood, 1986). The cytoskeletal and structural morphology of the germinating rhizoid is proposed to be reinforced by plasma membrane–cell wall links via vitronectin-like molecules in the cell wall linked to an intregrin-based, axis-stabilizing complex in the plasma membrane (Goodner and Quatrano, 1993). These links probably correspond to cytoplasmic adhesions exposed during

plasmolysis (see Figure 8B). Coordinate development of turgor with intracellular and extracellular asymmetries is likely to result in a localized mechanical transduction to the mechanosensitive channels present at the rhizoid tip—more so than those in subapical or thallus regions.

The data presented here show that the rhizoid tip region expands more than does any other region of the zygote during hypoosmotic shock. The apically localized Ca^{2+} gradient is absent when cell tugor is reduced by maintaining the zygote in a hyperosmotic medium, and large, apically localized Ca^{2+} transients occur in response to hypoosmotic-induced swelling. These transients originate at the extreme rhizoid apex and spread in a wavelike manner to subapical regions. Tension is also likely to be exerted on the rhizoid plasma membrane during plasmolysis by pulling it away from the cell wall at adhesion points. This process also induces transient elevations in cytoplasmic Ca^{2+}. Taken together, these results support our hypothesis that localized activation rather than asymmetric distribution of Ca^{2+}-permeable channels can maintain localized $[Ca^{2+}]_{cyt}$ elevations in the Fucus rhizoid. Thus, although the current data do not preclude the asymmetric distribution of a channel type not detected in this study, localized Ca^{2+} signaling, at least in the polarized rhizoid apex, can be explained in terms of localized activation of uniformly distributed channels.

To avoid $[Ca^{2+}]_{cyt}$ overload and membrane depolarization with such an abundant Ca^{2+}-permeable channel, it is likely that Ca^{2+} permeability is regulated in the intact zygote such that Ca^{2+} influx is minimized under typical physiological conditions. Run-down of channel activity after excision suggests that channel behavior is modulated not only by mechanical stress and voltage but also by cytosolic factors. Ca^{2+} permeability of the cation channel may be regulated in the following ways. (1) $[Ca^{2+}]_{cyt}$ and $[Ca^{2+}]_{ext}$ may regulate channel permeability as described in the guard cell K^+ inward rectifier channels (Fairley-Grenot and Assmann, 1992) and in *Chara* (Tester and MacRobbie, 1990). (2) SACs may adapt to mechanical stress. This may involve interactions with the cytoskeleton such that activity is relatively low under steady state turgor conditions. Channel activity may adapt to increases in turgor over time, which is a common feature of SACs in animal and yeast systems (Hamill and McBride, 1992). (3) Channel activity may be regulated by other cytoskeletal or cytoplasmic factors, such as actin polymerization or channel phosphorylation state (Suzuki et al., 1993; Allen and Sanders, 1995).

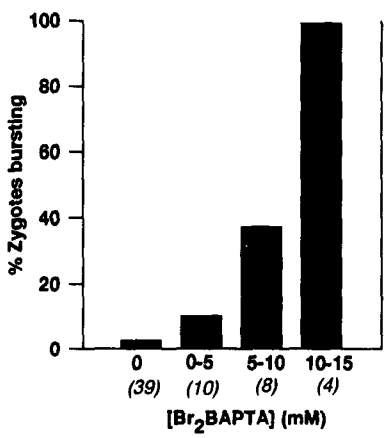

Figure 11. Effect of Intracellular [Br_2BAPTA] on the Ability of Rhizoid Cells to Osmoregulate in Response to Hypoosmotic Shock.

Rhizoid cells in ASW plus 0.7 M sorbitol were microinjected with varying intracellular [Br_2BAPTA] plus fura-2–dextran, followed after >1 hr by bath perfusion with ASW. The percentage of microinjected cells in each intracellular [Br_2BAPTA] range that burst in response to hypoosmotic shock is shown. Numbers of cells for each treatment are given within parentheses. Control injections (0 mM Br_2BAPTA) consisted of intracellular solution plus fura-2–dextran.

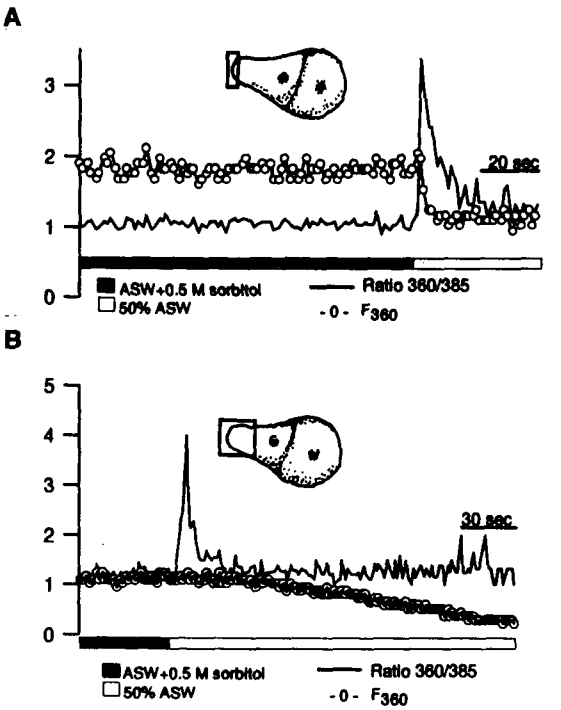

Figure 12. Simultaneous Measurement of a Ca^{2+} Transient and Ca^{2+} Influx in Response to Hypoosmotic Shock (ASW plus 0.5 M Sorbitol to ASW).

Ca^{2+} influx was monitored by the quenching of fura-2 fluorescence at 360 nm due to Mn^{2+} influx through Ca^{2+}-permeable channels. Boxes in **(A)** and **(B)** define regions from which recordings were made.
(A) Extreme rhizoid apex (10 μm) showing Ca^2 influx, monitored by fura-2 fluorescence at 360 nm excitation (F_{360}), coincident with the onset of the Ca^{2+} transient.
(B) Apical 30 to 40 μm. In this configuration, the fluorescence signal is predominantly from the rhizoid region behind the extreme apex (0 to 40 μm). Ca^{2+} influx is detectable only after the Ca^{2+} transient has expired.

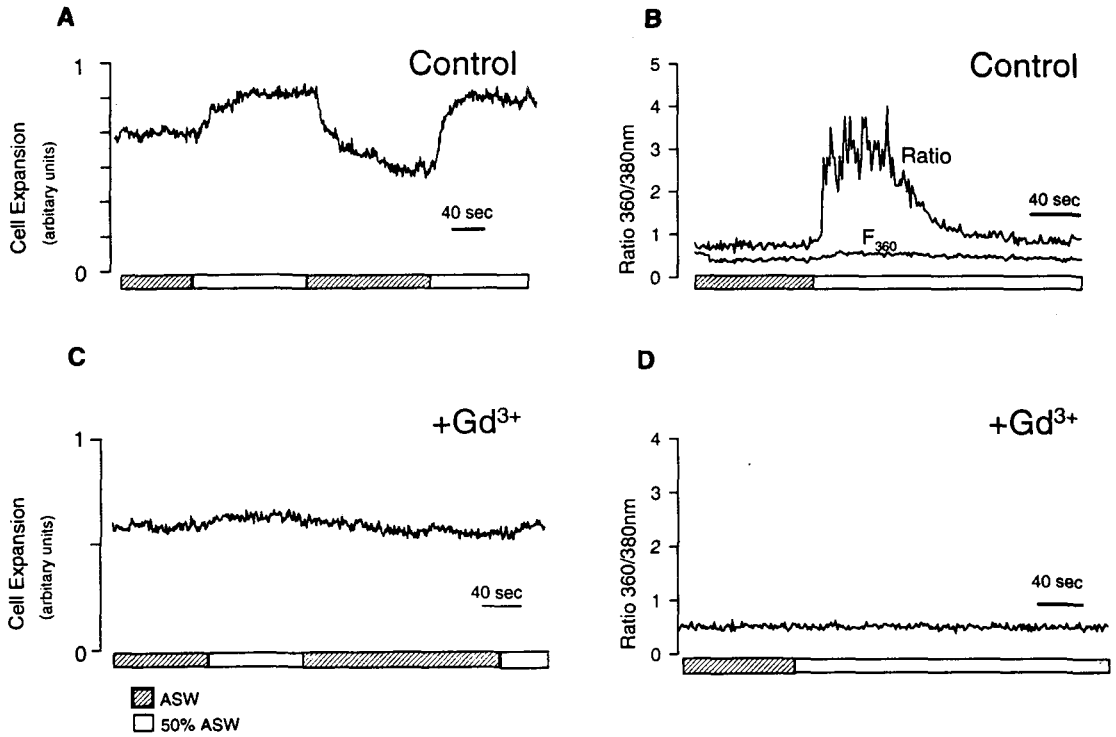

Figure 13. Effect of Gd^{3+} on Osmotically Induced Cell Volume Changes and a Ca^{2+} Transient in Response to Hypoosmotic Shock.

(A) Cell volume changes monitored continuously (see Methods) in the apical (20 μm) rhizoid region of a control cell. Transfer to hypoosmotic solution (from ASW, with HCO_3^- and SO_4^{2-} substituted with Cl^-, into 50% ASW) produced a small transient increase in cell volume. Transfer back to ASW caused a significant decrease in cell volume to less than the initial volume.

(B) A normal Ca^{2+} transient in response to the same hypoosmotic shock as given in **(A)**. Fura-2 fluorescence at the isosbestic point (F_{360}: 360 nm excitation) during the Ca^{2+} transient is also shown.

(C) Reduced magnitude and rate of cell volume increase and inhibition of volume decrease in response to the same hypoosmotic shock as given in **(A)** in the presence of 3 mM Gd^{3+} in the extracellular solution. Note the scale bar difference between **(A)** and **(C)**.

(D) Inhibition of the Ca^{2+} transient by 3 mM Gd^{3+} in the extracellular solution.

Sources of Ca^{2+} during Hypoosmotic Shock

The refractory period between two successive hypoosmotic shocks during which further Ca^{2+} transients cannot be elicited suggests either the occurrence of desensitization of the pathway involved in the elevation of Ca^{2+} or depletion of the source of Ca^{2+}. Desensitization of Ca^{2+} transients in response to repetitive touch stimuli has been observed in tobacco seedlings (Knight et al., 1991), where the source of Ca^{2+} appears to be intracellular (Knight et al., 1992). Desensitization of inositol 1,4,5-trisphosphate– and cyclic ADP-ribose–releasable intracellular Ca^{2+} stores has been described for sea urchin oocytes with refractory periods similar to those described in this study (Galione et al., 1991; Shen and Buck, 1993). $[Ca^{2+}]_{cyt}$ transients in response to hypoosmotic treatment have been observed in Lamprothamnium (Okazaki et al., 1987) and Nitella (Tazawa et al., 1995). In Nitella, the $[Ca^{2+}]_{cyt}$ increase was shown to arise from intracellular stores in response to cytoplasmic hydration (Tazawa et al., 1995). In pollen tubes, Ca^{2+} influx is responsible for generation of the apically located Ca^{2+} gradient (Pierson et al., 1994; Malhó et al., 1995). Both intracellular stores and Ca^{2+} influx are involved in the generation and propagation of the Ca^{2+} transient in the Fucus rhizoid.

Mn^{2+} has been used as a tracer for channel-mediated Ca^{2+} influx in a variety of animal cells (e.g., see Sage et al., 1989; Kass et al., 1990; Fasolata et al., 1993) and more recently in plant cells (Malhó et al., 1995; McAinsh et al., 1995) and Fucus eggs (Roberts and Brownlee, 1995). The technique is based on the observations that Mn^{2+} can permeate Ca^{2+} channels, has a very high binding affinity for fura-2 (K_d = 2 nM), and, on binding, quenches fura-2 fluorescence (Kwan and Putney, 1990) when monitored at the isosbestic excitation wavelength (360 nm). Single-channel recordings show that the Ca^{2+}-permeable channels in this study have low but finite permeability for Mn^{2+} and are not blocked by Mn^{2+}. Experiments utilizing Mn^{2+} quenching of fura-2 fluorescence to report Ca^{2+} influx show that in the extreme rhizoid apex, sig-

nificant rapid Ca^{2+} influx can be detected coincident with the onset of Ca^{2+} elevation. In more subapical regions, however, Ca^{2+} influx was not detected during the Ca^{2+} transient. Instead, a steady influx occurred after the cessation of the transient. This observation strongly suggests that Ca^{2+} elevation is initiated by Ca^{2+} influx at the rhizoid apex but propagates to subapical regions via release from intracellular stores. The Ca^{2+} influx detected after the Ca^{2+} transient in subapical regions may reflect the prolonged opening of channels allowing Ca^{2+} influx and K^+ efflux or elevated Ca^{2+} influx associated with recharging of intracellular Ca^{2+} stores. Elevated $[Ca^{2+}]_{cyt}$ would not be detected during this slow influx phase because incoming Ca^{2+} would be subject to rapid buffering, including uptake into intracellular stores. Thus, in addition to spatial control of plasma membrane channel activation, an additional level of organization of Ca^{2+} signaling appears to operate in the form of spatial localization or activation of intracellular Ca^{2+} stores.

Ca^{2+} Transient and Osmoregulation

Experiments in which osmolarity of the medium was changed under constant salinity (i.e., Figure 6) show that the responses reported here are elicted by changes in the osmotic environment alone. The reduced number of cells able to osmoregulate in a population of zygotes subjected to two successive hypoosmotic shocks correlates well with the refractory period for generation of a second Ca^{2+} transient. Furthermore, microinjection of the Ca^{2+} buffer Br_2BAPTA (K_d for Ca^{2+} = 3.6 μM) to concentrations that would effectively buffer Ca^{2+} elevations in the micromolar range (Speksnijder et al., 1989; Roberts et al., 1994) also reduced the ability of the rhizoid cell to osmoregulate. Thus, failure to generate a Ca^{2+} transient increases the probability of cell bursting. An essential role for cytoplasmic Ca^{2+} in transduction of signals involved in cell volume regulation is thus evident. A transient increase in cell volume during hypoosmotic shock, followed by a significant decrease in cell volume upon return to normal ASW, indicates the occurrence of solute or ion loss during acute osmoregulation. We propose that the transient $[Ca^{2+}]_{cyt}$ elevation triggers this loss by activation of Ca^{2+}-sensitive ion efflux channels. The increases in cell surface area (up to 20%) in the rhizoid apex cannot be accounted for by the purely mechanical stretch of the plasma membrane. Either the membrane is not fully extended within the cell wall or new membrane is reversibly inserted into the plasma membrane during swelling. Evidence for the latter has been provided by electron microscopy studies of vesicle fusions with the plasma membrane during hypoosmotic shock (Gilkey and Staehelin, 1989) in the related alga Pelvetia. Ca^{2+}-dependent exocytosis has been observed in other plant systems (e.g., see Zorec and Tester, 1992). It remains to be seen whether the Ca^{2+} transients involved in our study are involved in transient stimulation of exocytosis at the rhizoid apex.

Gd^{3+} blocks the mechanosensitive channels and inhibits the Ca^{2+} transient. However, Gd^{3+} reduced rather than increased the incidence of cell bursting in response to hypoosmotic shock. This osmoprotective effect of Gd^{3+} is due to the inhibition of osmotic swelling, reflecting inhibition of water movement into and out of the cell. It remains to be seen whether this alteration is due to direct blockage of water channels in the plasma membrane or to some other less specific effect on water movement. Nevertheless, these results imply that caution should be exercised in the interpretation of experiments in which Gd^{3+} is used as a specific ion blocker—particularly Ca^{2+} channels.

As an intertidal alga, Fucus regularly experiences very wide fluctuations in its ionic and osmotic environment. The restriction of this signal transduction pathway to the rhizoid cell may reflect the inability of this cell to generate large turgor pressures due to the thinner and less rigid cell wall and the need to carefully regulate cell volume to prevent cell bursting. Thallus cells have thicker, more rigid cell walls, enabling turgor generation and a reduced requirement for osmoregulation based on ion efflux. The restriction of this Ca^{2+} signal transduction mechanism to the rhizoid apex clearly shows that the interaction among differential mechanical properties of the cell wall, plasma membrane ion channels, and intracellular stores can pattern signal transduction. A variety of higher plant cell types (e.g., root hairs and pollen tubes) experience large fluctuations in their osmotic environment. It will be of great interest to discover whether similar mechanisms for spatial localization of Ca^{2+} signals are operative in other plant systems.

METHODS

Growth of Zygotes

Thallus tips bearing mature conceptacles of the monecious *Fucus spiralis* and dioecious *F. serratus* were collected, washed, and stored at 4°C in the dark. Zygotes of *F. spiralis* or *F. serratus* were obtained as described previously (Taylor and Brownlee, 1992; Berger and Brownlee, 1995). Zygotes were washed and placed in small Petri dishes with a glass cover slip base, incubated at 17°C in unidirectional white light (50 μmol m^{-2} sec^{-1}) to promote polarization, and used in both patch-clamp and cytoplasmic calcium $[Ca^{2+}]_{cyt}$ measurement experiments at the two-cell stage (18 to 24 hr).

Localized Protoplast Isolation with UV Laser

A pulsed nitrogen UV laser (VSL 337; Laser Science Inc., Cambridge, MA) was coupled to an inverted microscope (Nikon Diaphot 300; Nikon, Tokyo, Japan), via the UV epifluorescence port with beam-expanding optics (Spindler and Hoyer, Gottingen, Germany), assembled in the laboratory such that the UV beam was introduced into the microscope objective (Nikon UV-fluor ×40, numerical aperture of 1.3). The UV beam was focused to a spot (<1 μm), and the intensity was varied by use of neutral density filters (Spindler and Hoyer) so that the spot would

cut the zygote cell wall with a few pulses. Zygotes were plasmolyzed using artificial seawater (ASW) supplemented with 0.8 to 1.5 M sorbitol. The cell wall was perforated with the focused laser in cells in which plasmolysis had caused the plasma membrane to recede. Application of gentle mechanical pressure with a polished glass electrode or reducing the osmolarity of the medium enabled isolation of plasma membrane–bound protoplasts through perforations in both thallus and rhizoid locations (see Figure 1). Both *F. spiralis* and *F. serratus* were used in patch–clamp experiments according to availability. No significant difference in channel characteristics or $[Ca^{2+}]_{cyt}$ responses were detected between the two species.

Patch Clamping and Data Analysis

Cell-attached and excised single-channel recordings were made from apical, subapical, and thallus subprotoplasts by using conventional patch–clamp techniques (Hamill et al., 1981). The reference electrode consisted of an Ag/AgCl pellet in a holder containing the pipette solution and was connected to the bath via a 3% agar bridge made up of pipette medium. Patch pipettes were manufactured from thin-walled boroscillicate glass (GC150TF; Clark, Pangbourne, UK) on a Narishige puller (P-833; Narishige, Tokyo, Japan) and fire-polished on a laboratory-constructed microforge. Polished electrodes were briefly dipped in a 0.001% poly-L-lysine solution (Sigma) immediately before back-filling with ultrafiltered pipette solutions (0.22 μm; Millipore, Watford, UK). This simple treatment enhanced seal formation. Patch pipettes were connected via a pipette holder to the headstage of a patch–clamp amplifier (Axopatch 1D; Axon Instruments, Foster City, CA). Positive pressure was applied to the pipette via a water-filled manometer until the pipette was observed to touch the protoplast. Occasionally, gentle suction (<0.5 kPa) was required to promote seal formation. Bath solutions were exchanged using a simple gravity-fed input and suction output. Chamber volume was 0.5 cm^3, and perfusion rates were varied from 1 to 5 $cm^3\ min^{-1}$. Patch–clamp currents were filtered (1 or 2 kHz 4 pole Bessel), stored on video tape, and sampled using an analog-to-digital converter (Labmaster; Axon Instruments) driven by a personal computer and analyzed with Pclamp software (Axon Instruments). The probability of opening (P_{open}) at any voltage was determined using the all-points amplitude histograms (Bertl and Slayman, 1990) according to the formula

$$P_{open} = A_1 + 2A_2 \ldots + nA_n/n(A_0 + A_1 + \ldots A_n),$$

where A_0 represents the area under baseline or the closed peak representing the total time that all channels are closed, and A_1, A_2, to A_n are the areas under the peaks for each open level. A Boltzmann curve was fitted according to the equation $P_{open} = P_{open}^{max}/(1 + \exp(V_{mem} - V_{0.5})/S)$, where P_{open}^{max} is the maximum open probability and $V_{0.5}$ is the voltage at which P_{open} is half maximal. The slope factor S determines how steeply the activation curve changes with V_{mem} and is equivalent to $RT/\delta F$, where δ corresponds to the elementary gating charge, R is the gas constant, T is the absolute temperature, and F is the Faraday constant.

Patch–Clamp Solutions

In all excised patch–clamp experiments, the bath (cytosolic) solution contained 200 mM K^+-glutamate, 2 mM EGTA, 1 M sorbitol, and 10 mM Hepes, pH 7.8, adjusted with a Tris base. The free $[Ca^{2+}]$ in the cytosolic solutions was estimated to be 5 nM, based on calculations and titration of fura-2–containing solutions with Ca^{2+}. The concentrations of $[Ca^{2+}]$ and $[K^+]$ were varied in pipette solutions to test channel permeability (see Table 1). All media were made with 10 mM Hepes, pH 7.8, and had a Tris base. Ion activities (α_{ion}) for bath and pipette solutions are given in Table 1 and were calculated by multiplying the ion concentration by the ion activity coefficient (γ_{ion}). Values for γ_{ion} were calculated using the Debye-Huckel equation extended to account for divalent ions (Butler, 1968). Corrections were made for liquid junction potentials between the bath solution and the agar reference electrode (LJP_{ref}). LJP was measured or calculated so that the actual potential across the excised patch could be determined using the relationship $V_{mem} = -V_{pipette} + LJP_{ref}$ (Barry and Lynch, 1991; Neher, 1992). LJP values were calculated for all solutions using values for α_{ion} (Table 1). Permeability ratios for divalent and monovalent cation mixtures were determined from an extended Goldman Hodgkin and Katz constant field equation for channels that can conduct both monovalent and divalent cations (Jan and Jan, 1976). A simplified equation was used when only K^+ and Ca^{2+} were considered (Fairley-Grenot and Assmann, 1992).

Pressure Injection of Fura-2-Dextran for $[Ca^{2+}]_{cyt}$ Measurement and Imaging

F. serratus zygotes were pressure injected with 10,000 molecular weight dextran–linked fura-2, a dual excitation Ca^{2+}-sensitive dye (final intracellular concentration is ~50 μM; Roberts et al., 1994). The dye does not compartmentalize into intracellular organelles (Berger and Brownlee, 1993) and only reports cytoplasmic Ca^{2+}. Pipettes were fabricated from 1.2-mm filamented borosilicate glass (GC120F; Clark, Reading, UK) on a microelectrode puller (Kopf model 750; Kopf Instruments, Tujunga, CA) and dry beveled (Kaila and Voipio, 1985) before back filling with 1.0 mM fura-2–dextran in an intracellular solution (200 mM KCl, 5 mM $MgCl_2$, 5 mM Tris base, 100 mM EGTA, and 100 mM mannitol, pH 7.5). The micropipette was connected to a pressure microinjection unit (Picoinjector PL1-100; Medical System Corp., Greenville, NY). Back pressure of +20 kPa was applied to the pipette at all times to prevent any back filling by the extracellular solution or cytoplasm. Zygotes were placed in a hyperosmotic solution (0.5 M sorbitol in ASW) before impalement 20 μm from the tip of the germinating rhizoid. After impalement, the dye was introduced with up to eight pulses of 90 sec in duration at a pressure of +300 kPa. Injected zygotes were allowed to recover for at least 1 hr before commencing $[Ca^{2+}]_{cyt}$ measurement.

Ca^{2+} Buffer Microinjection

Rhizoid cells were coinjected with fura-2 and (Br_2BAPTA), using the protocol described above but with pipette solutions containing 50 mM Br_2BAPTA (Roberts et al., 1994). The final intracellular buffer concentration was estimated by measuring intracellular fura-2 fluorescence at 360 nm excitation (Ca^{2+} independent) and comparing this with a calibration curve of fluorescence of droplets containing known dye/buffer concentrations extruded from the injection pipette into silicon oil on a cover slip, using the same pulse protocol as was given for microinjection (Roberts et al., 1994).

Ratio Photometric $[Ca^{2+}]_{cyt}$ Measurements

Ca^{2+}-dependent fura-2 fluorescence was monitored using dual wavelength fluorescence microscopy with an inverted microscope (Nikon) using a ×40 oil immersion objective (1.3 n.a.; Nikon). Excitation wavelengths of 350 and 380 nm were generated by a rotating filter holder (UV line filters, 8 nm in bandwidth; Ealing Electro-Optics, Watford, UK) coupled via fiber optics to a 150-W xenon lamp. Fluorescence emission was detected by a photomultiplier tube (PM9924b; EMI, Hayes, UK) through a 520- to 560-nm bandwidth filter (Nikon). The photomultiplier output was synchronized with the excitation source by a microcomputer, using programs developed with Labview software (National Instruments Inc., Austin, TX). Autofluorescence of each region of the zygote monitored was recorded and subtracted on line from the fluorescence signal during experiments. Fluorescence signals at each excitation wavelength and calculated fluorescence ratios were displayed and recorded to disk at a rate of one fluorescence ratio per second. Ratio values (350/380 nm) were calibrated with respect to free $[Ca^{2+}]$ by comparison with ratios obtained with Ca^{2+} buffers containing 50 μM fura-2–dextran and by obtaining ratio values for Ca^{2+}-bound and Ca^{2+}-free fura-2 from dye-loaded cells (Roberts et al., 1994).

Ratio Imaging of $[Ca^{2+}]_{cyt}$

Fluorescence images of *F. serratus* zygotes microinjected with 10 to 50 μM fura-2–dextran were obtained with a 12-bit cooled CCD camera (Digital Pixel Ltd., Brighton, UK) and a personal computer using image acquisition programs developed with Labview software (National Instruments). Images were acquired at a rate of one image every 2 sec. Excitation and emission wavelengths were as described for Ca^{2+} photometry (see above). Autofluorescence was determined before microinjection and subtracted from fluorescence images as required. However, in most cases, autofluorescence represented <5% of dye fluorescence. Images were corrected for background fluorescence and camera dark current before performing ratio imaging. Ratio images (350/380 nm) were processed using Visilog (Noesis, Quebec, Canada) software running on a Silicon Graphics (Neuchartel, Switzerland) workstation. Pixel intensities of ratio images calibrated as was described for ratio photometry.

Mn^{2+} Quenching

Ca^{2+} influx during hypoosmotic treatment was monitored using the Mn^{2+}-quenching technique (Malhó et al., 1995; McAinsh et al., 1995; Roberts and Brownlee, 1995). Fura-2–dexran–loaded zygotes were incubated in ASW (with SO_4^{2-} replaced by Cl^-) containing 1.0 mM $MnCl_2$. Fura-2 fluorescence was monitored at 360 and 380 nm excitation. Entry of Mn^{2+} through Ca^{2+}-permeable channels quenches intracellular fura-2 fluorescence, which can be monitored as a decrease in signal at the isosbestic wavelength of 360 nm (Kwan and Putney, 1990; Fasolata et al., 1993). The 360/380–nm ratio was used to monitor changes in $[Ca^{2+}]_{cyt}$.

Osmotically Induced Changes in Cell Size

Zygotes adhering to the cover slip base of the perfusion chamber could be subjected to osmotic shock by rapidly changing the perfusion solution by using a gravity-fed perfusion system designed to allow a solution change within 1 sec of switching solutions. Changes in cell volume and surface area were monitored during photometric Ca^{2+} measurements by simultaneous bright-field (650 nm) and epifluorescence illumination of the cell. A 580-nm dichroic mirror in front of the photomultiplier allowed the bright-field image to be viewed by a CCD video camera (JVC, Tokyo, Japan). Changes in rhizoid and thallus cell length and diameter could be measured directly from video images. Precise kinetics of size changes in rhizoid cells during osmotic treatments were monitored in rhizoid cells by projecting a bright-field image of the apical 10 mm of the rhizoid apex onto a rectangular aperture (Nikon) in front of a photomultiplier. Expansion and contraction of the rhizoid caused the apex to move in and out of the diaphragm window with consequent increase or decrease in the absorbance of transmitted light.

ACKNOWLEDGMENTS

This research was supported by the Biotechnology and Biological Sciences Research Council (UK) Intracellular Signaling Programme and the Marine Biological Association of the United Kingdom. We thank Rémi Dumollard, Corrine Mercier, and Henrietta Stanley for their experimental help and Frederic Berger for valuable comment and discussion throughout the preparation of this manuscript.

Received February 13, 1996; accepted August 5, 1996.

REFERENCES

Alexandre, J., Lassalles, J.P., and Kado, R.T. (1990). Opening of Ca^{2+} channels in isolated beet root vacuolar membrane by inositol 1,4,5-trisphosphate. Nature **343,** 567–570.

Allen, G.J., and Sanders, D. (1994). Two voltage-gated, calcium release channels coreside in the vacuolar membrane of broad bean guard cells. Plant Cell **6,** 685–694.

Allen, G.J., and Sanders, D. (1995). Calcineurin, a type 2B protein phosphatase, modulates the Ca^{2+}-permeable slow vacular ion channel of stomatal guard cells. Plant Cell **7,** 1473–1483.

Allen, G.J., Muir, S.R., and Sanders, D. (1995). Release of Ca^{2+} from individual plant vacuoles by both InsP3 and cyclic ADP-ribose. Science **268,** 735–737.

Allen, R.D., Jacobsen, J.J., and Jaffe, L.F. (1970). Ionic concentrations in developing *Pelvetia* eggs. Dev. Biol. **27,** 538–545.

Barry, P.H., and Lynch, J.W. (1991). Liquid junction potentials and small cell effects in patch–clamp analysis. J. Membr. Biol. **121,** 101–117.

Berger, F., and Brownlee, C. (1993). Ratio confocal imaging of free cytoplasmic Ca^{2+} gradients in polarizing and polarized *Fucus* zygotes. Zygote **1,** 9–15.

Berger, F., and Brownlee, C. (1995). Physiology and development of protoplasts obtained from Fucus using laser microsurgery. Protoplasma **186,** 63–71.

Berger, F., Taylor, A.R., and Brownlee, C.B. (1994). Cell fate determination by the cell wall in early Fucus development. Science **263,** 1421–1423.

Bertl, A., and Slayman, C.L. (1990). Cation selective channels in the vacuolar membrane of *Saccharomyces*: Dependence on calcium, redox state, and voltage. Proc. Natl. Acad. Sci. USA **87,** 7824–7828.

Brownlee, C., and Wood, J.W. (1986). A gradient of free Ca^{2+} in growing rhizoid cells of *Fucus serratus*. Nature **320,** 624–626.

Butler, J.N. (1968). The thermodynamic activity of calcium ion in sodium chloride–calcium chloride electrolytes. Biophys. J. **8,** 1426–1433.

Cosgrove, D.J., and Hedrich, R. (1991). Stretch-activated Cl^-, K^+ and Ca^{2+} channels coexisting in plasma membranes of guard cells of *Vicia faba* L. Planta **186,** 143–153.

De Boer, A.H., van Duijn, B., Giesberg, P., Wegner, L., Obermeyer, G., Kohler, K., and Linz, K.W. (1994). Laser microsurgery: A versatile tool in plant (electro) physiology. Protoplasma **178,** 1–10.

Ding, P.J., and Pickard, B. (1993). Mechanosensory Ca^{2+} selective cation channels in epidermal cells. Plant J. **3,** 83–110.

Fairley-Grenot, K.A., and Assmann, S.M. (1992). Permeation of Ca^{2+} through K^+ channels in the plasma membrane of *Vicia faba* guard cells. J. Membr. Biol. **128,** 103–113.

Fasolata, C., Hoth, M., Matthews, G., and Penner, R. (1993). Ca^{2+} and Mn^{2+} influx through receptor-mediated activation of nonspecific cation channels in mast cells. Proc. Natl. Acad. Sci. USA **90,** 3068–3072.

Feijo, J.A., Malhó, R., and Obermeyer, G. (1995). Ion dynamics and its possible role during in vitro pollen germination and tube growth. Protoplasma **187,** 155–167.

Galione, A., Lee, H.C., and Busa, W.B. (1991). Ca^{2+}-induced Ca^{2+} release in sea urchin egg homogenates: Modulation by cyclic ADP-ribose. Science **253,** 1143–1146.

Garrill, A., Lew, R.R., and Heath, I.B. (1992). Stretch-activated Ca^{2+} and Ca^{2+} activated K^+ channels in the hyphal tip plasma membrane of the oomycete *Saphrolegma ferax*. J. Cell Sci. **101,** 721–730.

Gibbon, B.C., and Kropf, D.L. (1994). Cytosolic pH gradients associated with tip growth. Science **263,** 1419–1421.

Gilkey, J.C., and Staehelin, A.L. (1989). A new organelle related to osmoregulation in ultrarapidly frozen *Pelvetia* embryos. Planta **178,** 425–435.

Gilroy, S., Bethke, P.C., and Jones, R.L. (1993). Calcium homeostasis in plants. J. Cell Sci. **106,** 453–462.

Goodner, B., and Quatrano, R.S. (1993). *Fucus* embryogenesis: A model to study the establishment of polarity. Plant Cell **5,** 1471–1481.

Gustin, C.M., Zhou, X.-L., Martinac, B., and Kung, C. (1986). Mechanosensitive ion channels in yeast plasma membrane. Science **233,** 1195–1197.

Hamill, O.P., and McBride, D.W. (1992). Rapid adaptation of single mechanosensitive channels in *Xenopus* oocytes. Proc. Natl. Acad. Sci. USA **89,** 7462–7466.

Hamill, O.P., Marty, E., Neher, E., Sakmann, B., and Sigworth, F.J. (1981). Improved patch-clamp techniques for high-resolution current recording from cells and cell-free membrane patches. Pflugers Arch. **391,** 85–100.

Henricksen, G.H., Taylor, A.R., Brownlee, C., and Assmann, S.M. (1996). Laser microsurgery of higher plant cell walls permits patch-clamp access. Plant Physiol. **110,** 1063–1068.

Hermann, A., and Felle, H. (1995). Tip growth in root hair cells of *Sinapis alba* L.: Significance of internal and external Ca^{2+} and pH. New Phytol. **129,** 523–533.

Jan, L.Y., and Jan, Y.N. (1976). L-Glutamate as an excitatory transmitter at the Drosophila larval neuromuscular junction. J. Physiol. **262,** 215–236.

Johannes, E., and Sanders, D. (1995). Lumenal calcium modulates unitary conductance and gating of an endomembrane calcium release channel. J. Membr. Biol. **146,** 211–224.

Johannes, E., Brosnan, J.M., and Sanders, D. (1992). Calcium channels in the vacuolar membrane of plants: Multiple pathways for intracellular calcium mobilisation. Philos. Trans. R. Soc. Lond. B **338,** 105–112.

Kaila, K., and Voipio, J. (1985). A simple method for dry bevelling of micropipettes in the construction of ion sensitive microelectrodes. J. Physiol. **369,** 8.

Kass, E.N., Llopis, J., Duddy, S.K., and Orrenius, S. (1990). Receptor-operated calcium influx in rat hepatocytes. J. Biol. Chem. **265,** 17486–17492.

Klüsener, B., Boheim, G., Lib, H., Engelberth, J., and Weiler, E.W. (1995). Gadolinium-sensitive, voltage-dependent calcium release channels in the endoplasmic reticulum of a higher plant mechanoreceptor organ. EMBO J. **14,** 2708–2714.

Knight, M.R., Campbell, A.K., Smith, S.M., and Trewavas, A.J. (1991). Transgenic plant aequorin reports the effects of touch and cold-shock and elicitors on cytoplasmic calcium. Nature **352,** 524–526.

Knight, M.R., Campbell, A.K., and Trewavas, A.J. (1992). Wind-induced plant motion immediately increases cytosolic calcium. Proc. Natl. Acad. Sci. USA **89,** 4967–4971.

Kropf, D.L. (1992). Establishment and expression of polarity in fucoid zygotes. Microbiol. Rev. **56,** 316–339.

Kropf, D.L. (1994). Cytoskeletal control of cell polarity in a plant zygote. Dev. Biol. **165,** 361–371.

Kropf, D.L., Berge, S.K., and Quatrano, R.S. (1989). Actin localization during *Fucus* embryogenesis. Plant Cell **1,** 191–200.

Kurkdjian, A., Leitz, G., Manigault, P., Harim, A., and Greulich, K.O. (1993). Non-enzymatic access to the plasma membrane of *Medicago* root hairs by laser microsurgery. J. Cell Sci. **105,** 263–268.

Kwan, C.-Y., and Putney, J.W. (1990). Uptake and sequestration of divalent cations in resting and methacholine-stimulated mouse acinar cells. J. Biol. Chem. **265,** 678–684.

Malhó, R., Read, N.D., Trewavas, A.J., and Pais, M.S. (1995). Calcium channel activity during pollen tube growth and reorientation. Plant Cell **7,** 1173–1184.

McAinsh, M.R., Webb, A.A.R., Taylor, J.E., and Hetherington, A.M. (1995). Stimulus-induced oscillations in guard cell cytosolic free calcium. Plant Cell **7,** 1207–1213.

Miller, D.D., Callaham, D.A., Gross, D.J., and Hepler, P.K. (1992). Free Ca^{2+} gradient in growing pollen tubes of *Lilium*. J. Cell Sci. **101,** 7–12.

Neher, E. (1992). Correction for liquid junction potentials in patch-clamp experiments. Methods Enzymol. **207,** 123–131.

Okazaki, Y., Yoshimoto, Y., Hiramoto, Y., and Tazawa, M. (1987). Turgor regulation and cytoplasmic free Ca^{2+} in the alga *Lamprothamnium*. Protoplasma **140,** 67–71.

Pantoja, O., Gelli, A., and Blumwald, E. (1992). Voltage-dependent calcium channels in plant vacuoles. Science **255,** 1567–1570.

Pierson, E.S., Miller, D.D., Callaham, D.A., Shipley, A.M., Rivers, B.A., Cresti, M., and Hepler, P.K. (1994). Pollen tube growth is cou-

pled to the extracellular calcium ion flux and the intracellular calcium gradient: Effect of BAPTA-type buffers and hypertonic media. Plant Cell **6,** 1815–1828.

Piñeros, M., and Tester, M. (1995). Characterisation of a voltage dependent Ca^{2+}-selective channel from wheat roots. Planta **195,** 478–488.

Poovaiah, B.W., and Reddy, A.S.N. (1993). Calcium and signal transduction in plants. Crit. Rev. Plant Sci. **12,** 185–211.

Rathore, K.S., Cork, R.J., and Robinson, K.R. (1991). A cytoplasmic gradient of Ca^{2+} is correlated with the growth of lily pollen tubes. Dev. Biol. **148,** 612–619.

Roberts, S.K., and Brownlee, C. (1995). Calcium influx, fertilisation potential and egg activation in *Fucus serratus.* Zygote **3,** 191–197.

Roberts, S.K., Berger, F., and Brownlee, C. (1993). The role of calcium in signal transduction following fertilization in *Fucus serratus.* J. Exp. Biol. **184,** 197–212.

Roberts, S.K., Gillot, I., and Brownlee, C. (1994). Cytoplasmic calcium and *Fucus* egg activation. Development **120,** 155–163.

Sage, O.S., Merritt, J.E., Hallam, T.R., and Rink, T.J. (1989). Receptor-mediated calcium entry in fura-2 loaded human platelets stimulated with ADP and thrombin. Biochem. J. **258,** 923–926.

Schroeder, J.I. (1989). Quantitive analysis of outward rectifying K^+ channel currents in guard cell protoplasts from *Vicia faba.* J. Membr. Biol. **107,** 229–235.

Schroeder, J.I., and Hagiwara, S. (1990). Repetitive increases in Ca^{2+} of guard cells by ABA elevation and non-selective Ca^{2+} permeable channel. Proc. Natl. Acad. Sci. USA **87,** 9305–9309.

Schroeder, J.I., and Thuleau, P. (1991). Ca^{2+} channels in higher plant cells. Plant Cell **3,** 555–559.

Shaw, S.L., and Quatrano, R.S. (1996). Polar localization of dihydropyridine receptor on living *Fucus* zygotes. J. Cell Sci. **109,** 335–342.

Shen, S.S., and Buck, W.R. (1993). Sources of calcium in sea urchin eggs during the fertilization response. Dev. Biol. **157,** 157–169.

Speksnijder, J.A., Miller, A.L., Weisenseel, M.H., Chen, T.-H., and Jaffe, L.F. (1989). Calcium buffer injections block fucoid egg development by facilitating calcium diffusion. Proc. Natl. Acad. Sci. USA **86,** 6607–6611.

Steer, J.M., and Steer, M.W. (1989). Calcium control of pollen tube tip growth. New Phytol. **111,** 323–358.

Suzuki, M., Miyazaki, K., Ikeda, M., Kawaguchi, Y., and Sakai, O. (1993). F-actin network may regulate a Cl^- channel in renal proximal tubule cells. J. Membr. Biol. **134,** 31–39.

Taylor, A.R., and Brownlee, C. (1992). Localized patch clamping of plasma membrane of a polarized plant cell; laser microsurgery of the *Fucus spiralis* rhizoid cell wall. Plant Physiol. **99,** 1686–1688.

Taylor, A.R., and Brownlee, C. (1993). Calcium and potassium currents in the *Fucus* egg. Planta **189,** 109–119.

Tazawa, M., Shimada, K., and Kikuyama, M. (1995). Cytoplasmic hydration triggers increase in cytoplasmic Ca^{2+} concentration in *Nitella flexilis.* Plant Cell Physiol. **36,** 335–340.

Tester, M., and MacRobbie, E.A.C. (1990). Cytoplasmic calcium affects the gating of potassium channels in the plasma membrane of *Chara corallina*: A whole cell study using calcium channel effectors. Planta **180,** 569–581.

Thuleau, P., Ward, J.M., Ranjeva, R., and Schroeder, J.I. (1994). Voltage dependent calcium permeable channels in the plasma membrane of higher plant cells. EMBO J. **13,** 2970–2975.

Ward, J.M., and Schroeder, J.I. (1994). Calcium-activated K^+ channels and calcium-induced calcium release by slow vacuolar ion channels in guard cell vacuoles implicated in the control of stomatal closure. Plant Cell **6,** 669–683.

Ward, J.M., Pei, Z.-M., and Schroeder, J.I. (1995). Roles of ion channels in initiation of signal transduction in higher plants. Plant Cell **7,** 833–844.

Zorec, R., and Tester, M. (1992). Cytoplasmic calcium stimulates exocytosis in a plant secretory cell. Biophys. J. **63,** 864–867.